AIAA 81-1878R

Analysis of Static and Dynamic Wind Tunnel Tests of the Shuttle Cable Trays

J. Peter Reding* and Lars E. Ericsson†
Lockheed Missiles and Space Company, Inc., Sunnyvale, Calif.

This article presents the results of a study aimed at determining the possible aeroelastic instability of the Space Shuttle cable trays. Cross flow over the trays, caused by unique flow interference effects, was found to be the potential source of the aeroelastic instability. Selected data from static and dynamic wind tunnel tests of cable tray sections, which furnished the essential input into the aeroelastic analysis, are presented and analyzed. The critical flow phenomena threatening the aeroelastic stability of the trays are shown to be sudden changes in the cross-flow-induced channel flow between the cable tray and the Shuttle external tank, which generate discontinuous aerodynamic characteristics. The search for a successful aerodynamic fix that prevented aeroelastic instability and structural failure of the trays is described.

Nomenclature

b = span (Fig. 9)
c = two-dimensional chord length (Fig. 9)
f = frequency
h = cross-sectional height of cable tray (Fig. 9)
Δh = gap size (Fig. 9)
ℓ = ground plane extent (Fig. 9)
l = sectional lift, coefficient $c_l = l/(\rho V^2/2)c$
M = Mach number
n = sectional normal force, coefficient $c_n = n/(\rho V^2/2)c$
p = static pressure, coefficient $C_p = (p-p_\infty)/(\rho V^2/2)$
q = pitch rate
Re = Reynolds number $= Vc/\nu$
r = corner radius
t = time
V = cross-flow velocity
$\bar{V}_d$ = mean downstream convection velocity
V_u = upstream shock velocity
α = angle of attack
γ = cross-flow angle, positive in the inboard direction
Δ = increment and amplitude
ν = kinematic viscosity of air
ρ = air density
τ = dimensionless time $= Vt/c$

Subscript

∞ = freestream condition

Superscript

i = separation induced, e.g., $\Delta^i c_n$ = separation-induced normal force

Derivative Symbols

$$c_{m_\alpha} = \frac{\partial c_m}{\partial \alpha}$$

$$c_{mq} = \frac{\partial c_m}{\partial (cq/V)}$$

$$c_{m_{\dot\alpha}} = \frac{\partial c_m}{(c\dot\alpha/V)} : c_{m_{\dot z}} = \frac{\partial c_m}{\partial (\dot z/V)}$$

$$\dot\alpha = \frac{\partial \alpha}{\partial t} : \ddot q = \frac{\partial^2 q}{\partial t^2}$$

Presented as Paper 81-1878 at the AIAA Atmospheric Flight Mechanics Conference, Alburquerque, N. Mex., Aug. 19-21, 1981; submitted Sept. 30, 1981; revision received Feb. 5, 1982.

*Staff Engineer. Associate Fellow AIAA.
†Senior Consulting Engineer. Associate Fellow AIAA.

Introduction

EARLY in 1979, a concern developed about the structural integrity of the Space Shuttle liquid oxygen (LO_2) cable tray (Fig. 1) because it had a very low structural margin. Because of previous experience,[1-3] the authors were retained as consultants for investigation of possible self-excited oscillations of the cable tray.

The study was conducted in three stages. First, the Shuttle flowfield was studied. It was shown that the LO_2 cable tray, of approximately rectangular cross section, was subjected to significant cross flow. Analysis of the initial LO_2 cable tray geometry in the cross flow induced by the solid rocket booster (SRB) showed that the structural integrity of the cable tray could not be assured.[4] Consequently, two-dimensional static[5] and dynamic[6] wind tunnel tests were conducted on the then current LO_2 and SRB cable tray sections, which differed substantially from the initial LO_2 cable tray geometry. These tests, which were to provide the needed input data for aeroelastic analysis of the cable trays, were conducted with a ground plane simulating the external tank (ET) surface.

Unfortunately, before the aeroelastic analysis could be completed, it was necessary to ensure that the cable trays on the first Shuttle flight did not fail. Thus an aerodynamic fix was designed that would prevent any potential aeroelastic problem.

This paper presents an analysis of the Shuttle interference flowfield that subjects the LO_2 cable tray and other cable trays to significant cross flow, briefly recapitulates the

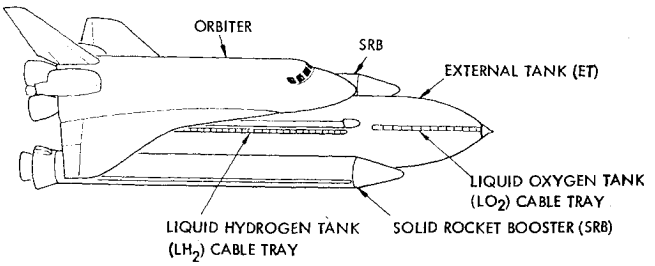

Fig. 1 Space Shuttle booster.

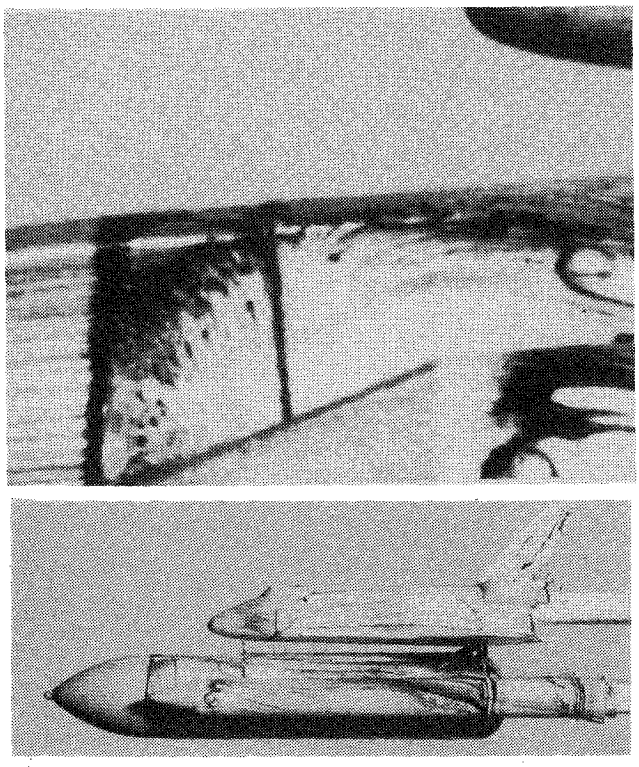

a)

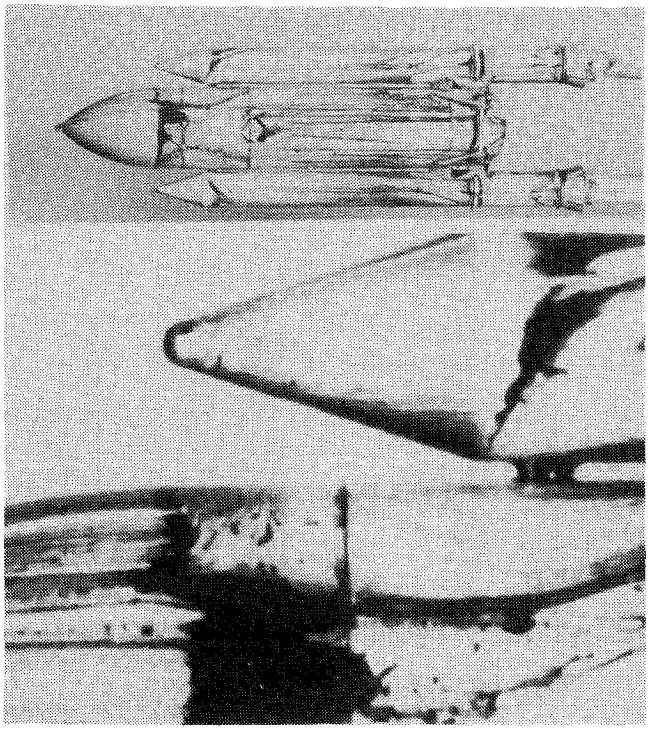

b)

Fig. 2 Interference flow patterns on the Shuttle booster; $M=1.1$, $\alpha=0$.

essential results of the initial aeroelastic analysis of the LO_2 cable tray discussed elsewhere,[4] and reviews the analysis of the static and dynamic wind tunnel data pertinent to the design of the aerodynamic fix.

Interference Flowfield

The parallel stage Space Shuttle launch configuration experiences several complicated flow interference effects, one of which causes the local flow on the ET to be normal and

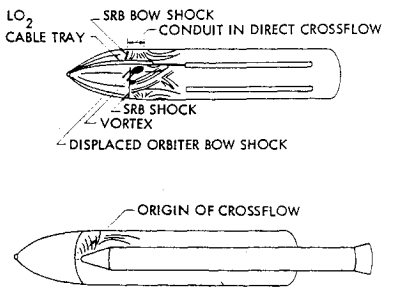

Fig. 3 Evidence of direct cross flow over conduit; $M=1.1$, $\alpha=0$.

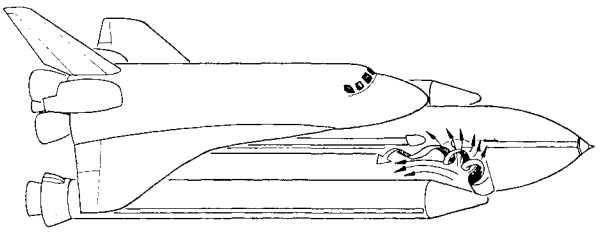

Fig. 4 SRB-ET interference flowfield.

even counter to the freestream direction. This strong interference effect is evident in the oilflow photographs in Fig. 2. These heretofore unpublished oilflow photographs were taken in the Marshall Space Flight Center (MSFC) 14-in. Trisonic Wind Tunnel by covering the model with oil dots and running the wind tunnel until the resulting oil streak patterns stabilized. The orbiter was then removed, and the ET/SRB flow patterns were photographed.

The oilflow photograph of the interference flowfield on the ET/SRB's at $M=1.1$ shows the trace of the displaced orbiter bow shock (see Fig. 2 and interpretive sketches in Fig. 3). It also shows a region of direct cross flow over the cable tray/gaseous oxygen pipe caused by the interference flow from the right SRB. The left profile of the booster provides another view of the interference flowfield. The interference regions can be seen more clearly in the inset blowups. The flow aft of the SRB bow shock fans out in all directions. Not only does it impinge normal to the LO_2 cable tray, but upstream flow is also evident, especially in the profile photograph.

This interference flow does not develop until a strong bow shock occurs forward of the SRB's, i.e., until $M>1.0$. The large adverse pressure gradient produced by the strong bow shock causes the ET boundary layer to separate, with reattachment occurring under the SRB nose cone. Thus upstream flow is produced in the recirculation region of the separation bubble. The separated region is vented above and below the SRB through a horseshoe vortex. It is the upper leg of the horseshoe vortex that induces the 90-deg crossflow over the LO_2 cable tray as it scrubs the ET surface while curving downstream (Fig. 4).

The LO_2 cable tray is located 31.5 deg off the leeward meridian of the ET. Thus top and side view photographs were used together to give a good average measure of the crossflow angle over the LO_2 cable tray.

The flow parameters at the cable tray were computed from pressure distribution and the boost trajectory data.[7] Freestream flow conditions were expanded to the local pressure at the appropriate cable tray station both isentropically and by accounting for normal shock losses as the flow passed through both ET and SRB bow shocks.

The LO_2 tray is not the only cable tray on the shuttle ET (Fig. 5). Cross-flow distributions over the ET indicate that the SRB trays experience large (70-deg) cross flow and the LH_2 tray also experiences significant ($\pm$20-deg) cross flow (Fig. 6).

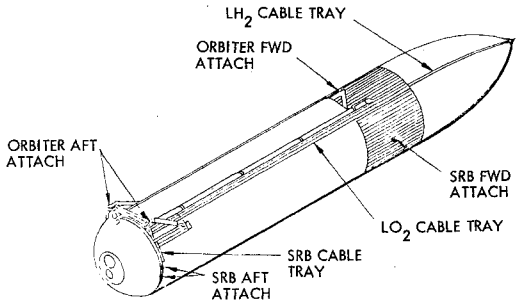

Fig. 5 Shuttle external tank configuration.

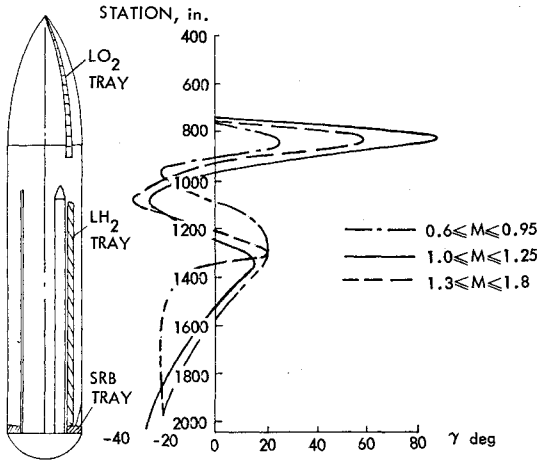

Fig. 6 Cross-flow distribution.

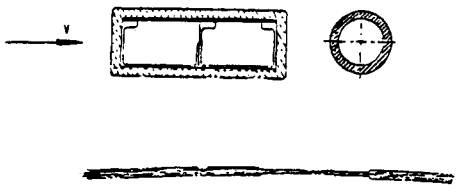

a) Actual cross-sectional geometry.

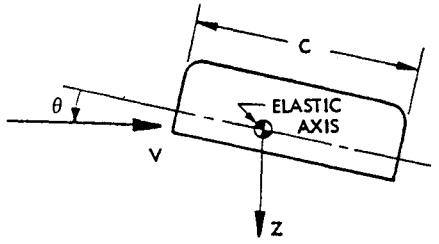

b) idealized cross-section.

Fig. 7 Early LO_2 cable tray.

Initial Aeroelastic Estimates

The early LO_2 cable tray configuration was rectangular with an adjacent circular gaseous oxygen pipe. Both were suspended above the ET tank surface on support legs (Fig. 7a). Because of the paucity of wall interference or ground plane data, the effect of the gaseous oxygen pipe and ET surface were neglected in the initial analysis‡ (Fig. 7b).

‡For the initial ground plane distance (Fig. 7a), this was probably a good assumption.

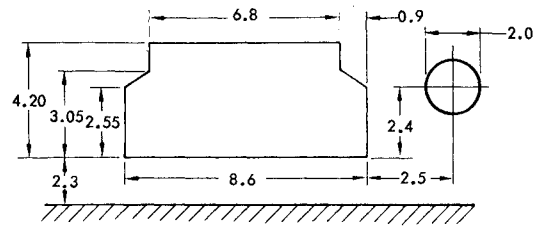

Fig. 8 LO_2 cable tray configuration for static test.

MSFC STATIC TEST

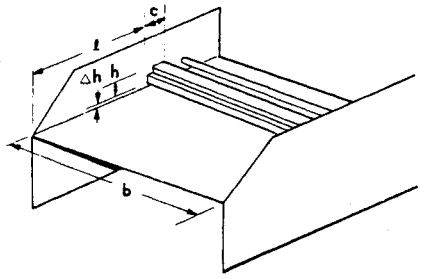

c = 1.032 IN. (LO_2)
c = 1.284 IN. (SRB)
h/c = 0.488
Δh/h = 0.55, 1.4
b/c = 5.814
ℓ/c = 0.783
M = 0.5 ≤ M ≤ 1.46
$0.6 \times 10^6 < R_e < 0.8 \times 10^6$

NAE DYNAMIC TEST

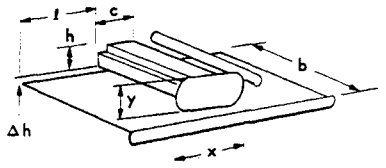

c = 1.968 IN.
h/c = 0.5
Δh/h = 0.55, 1.4
b/c = 2.4, 3.2
ℓ/c = 2.25
x/c = 1.3
y/h = 1.4
M = 0.21 ≤ M ≤ 0.92
$0.25 \times 10^6 < R_e < 0.8 \times 10^6$

Fig. 9 Comparison of wind tunnel test setups.

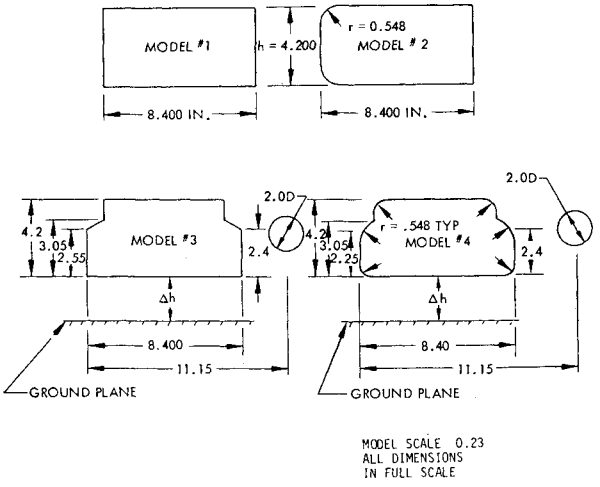

Fig. 10 Cable tray configuration for dynamic tests.

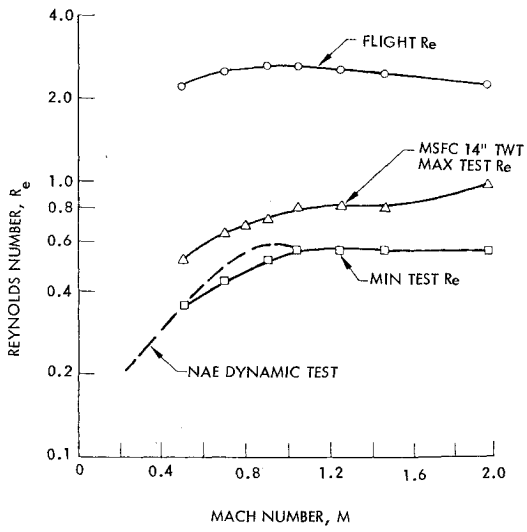

Fig. 11 Reynolds number comparison.

Nakamura and Mizota have shown that the flow is separated over rectangular sections even at low subsonic speeds.[8] Experience with flat-faced cylinders shows[9] that the separation can only increase at high subsonic speeds. Thus flow separation will dominate the aerodynamics of the LO_2 tray over much of the flight.

The separation-induced statically stabilizing moment characteristics of rectangular cross sections measured by Nakamura and Mizota[8] give concern for the aeroelastic stability of torsional oscillations. The loads in the separated flow region do not occur instantaneously, but lag the motion because of the finite flow convection speed in the separated region. This time lag causes statically stabilizing aerodynamic loads to be dynamically destabilizing.[1-4] Thus, in the case of the separated flow on the cable tray, the statically stabilizing aerodynamic load is destabilizing dynamically.

The damping of both bending and torsional modes of the LO_2 cable tray were estimated using analytic techniques that account for the flowfield time lag.[4] The estimated aerodynamic undamping exceeded the structural damping for the two lowest torsional modes at subsonic cross-flow Mach numbers, indicating the possibility of structural failure resulting from undamped torsional oscillations. Likewise, structural failure was also predicted for the sudden flow separation that occurs for $M>1.0$, causing excessive limit cycle oscillations of both bending and torsional modes. Thus it was decided that a more accurate analysis, which used experimental results for the actual cable tray cross section in the presence of the ET surface, must be conducted.

Wind Tunnel Tests

The static test consisted of static pressure measurements integrated to give static stability coefficients on sections of the then current LO_2 cable tray with sharp edges[5] (Fig. 8). The model was mounted in an end-plated channel in the MSFC 14-in. Trisonic Wind Tunnel (Fig. 9) to give two-dimensional data in the presence of a ground plane simulating the ET. The dynamic data, measured in the dynamics tunnel at the National Research Council of Canada, Ottawa, Canada, were taken on two-dimensional rectangular and LO_2 cable tray sections that simulated the possible extremes in the corner radius of the thermal protection material that covered the cable trays (Fig. 10). These end-plated sections (Fig. 9) were tested with and without a ground plane and with ground plane gaps simulating both LO_2 and SRB cable tray standoffs. The testing of the rectangular sections and the testing without a ground plane were included to help bridge the gap between the earlier estimates and the simulated effects of the ET surface.

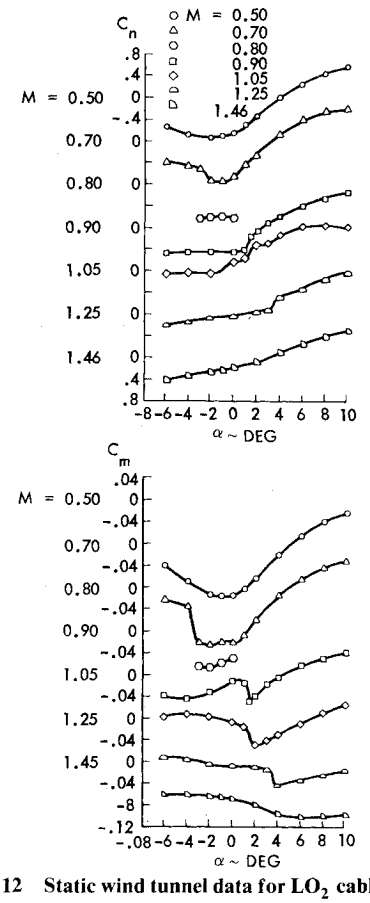

Fig. 12 Static wind tunnel data for LO_2 cable tray.

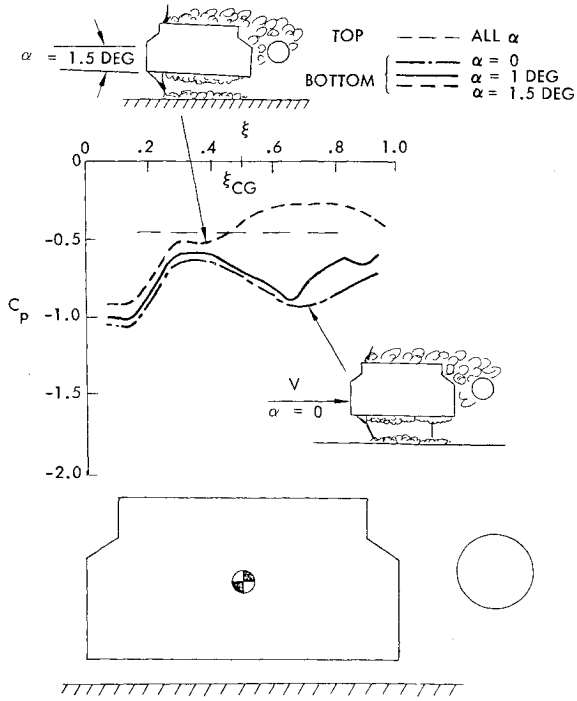

Fig. 13 Static pressure distribution on the LO_2 cable trays at $M=0.9$.

The Reynolds numbers compared well between the two tests but were well below the flight values (Fig. 11).

Static Tests

The static data showed stabilizing discontinuities in C_m at 2 deg $\leq\alpha\leq$4 deg for $0.9\leq M\leq 1.25$ and at $\alpha=-4$ deg for $M=0.7$ for the LO_2 cable tray (Fig. 12). These stabilizing

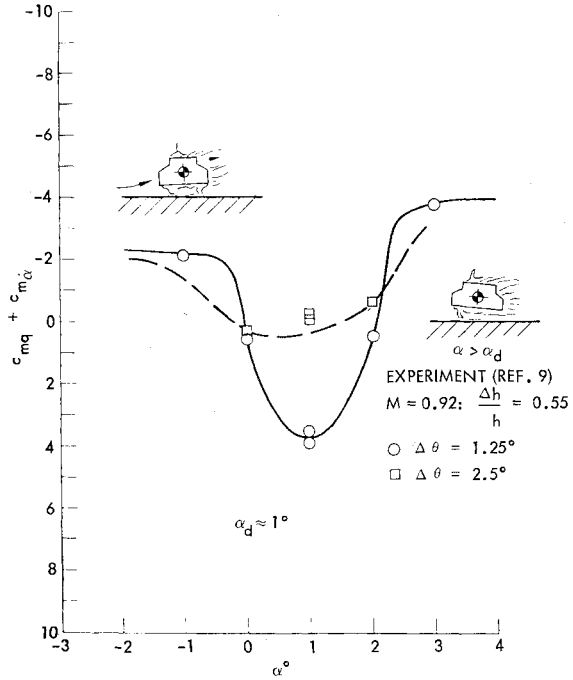

Fig. 14 Effect of flow discontinuity on the dynamic stability of the LO_2 cable tray at $M = 0.92$.

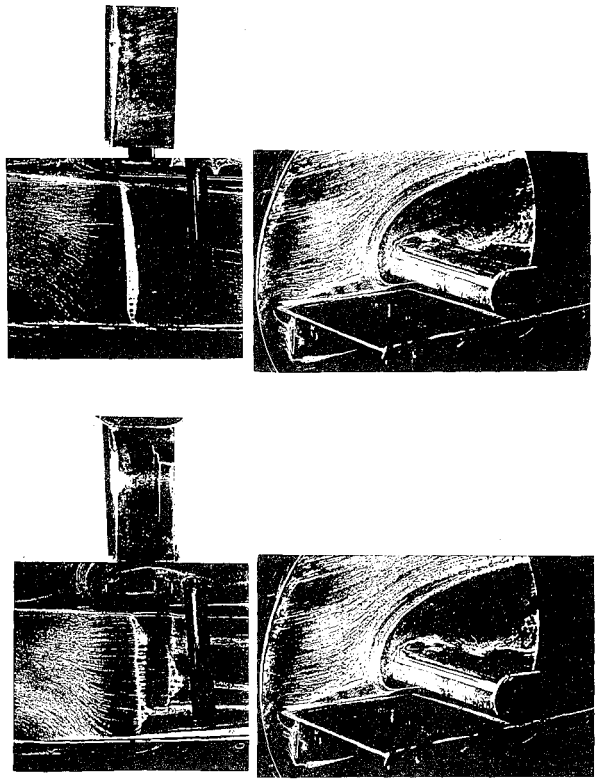

Fig. 15 Oilflow photographs for dynamic models. $\alpha = 2$ deg. $\alpha = 0$.

discontinuities in the static stability characteristics cause destabilizing discontinuities in the dynamic stability because of the flowfield time lag effects discussed earlier. This will result in limit cycle oscillations of the structure.[10-13]

The pressure distribution data reveal the causes of these discontinuities. At $M = 0.9$, it is the sudden merging of two shocks in the channel between the cable tray bottom and the ground plane (Fig. 13). The channel between the cable tray and the ground plane acts like a sonic throat. The flow entering the inlet is reaccelerated to supersonic speed. This local

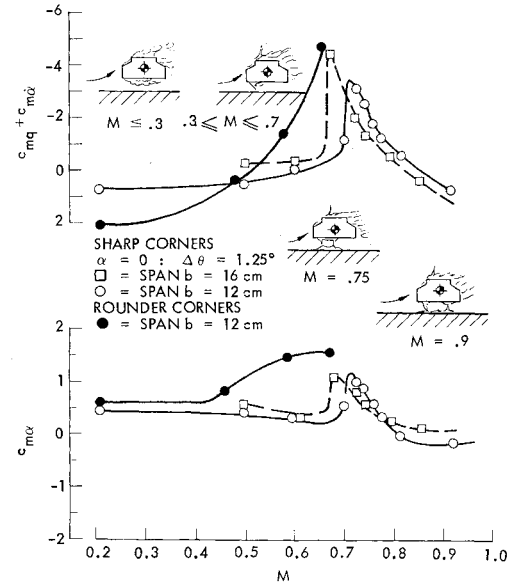

Fig. 16 Unsteady aerodynamic characteristics $\alpha = 0$ of the LO_2 cable tray.

supersonic region is terminated by a strong shock that generates a sudden pressure rise and an associated flow separation bubble. At $\alpha = 1$ deg, the flow separation bubble again constricts the flow acting as a second sonic throat, reaccelerating the flow to supersonic speed. This second supersonic region is terminated by another strong shock that provides the pressure rise back to the base pressure level. When the cable tray is pitched from 1 to 1.5 deg, the channel exit area is constricted enough to force the second shock to jump forward to merge with the first shock. The resulting gross flow separation causes a completely subsonic flow behavior down the channel to the exit. The shock jump generates a discontinuous increase of the bottom-side pressures, resulting in a positive normal force discontinuity (Δc_n) and a corresponding stabilizing pitching moment discontinuity ($-\Delta c_m$) because the positive pressure jump occurs aft of the rotation center (Fig. 13).

The cause of the discontinuity at $M = 0.7$ and $\alpha \approx -4$ deg is discussed in Ref. 11. This is not of concern to the LO_2 cable tray, as the curvature of the LO_2 tank puts the cable tray at a positive 3-deg angle of attack.

Dynamic Data

The dynamic data show an amplitude sensitive undamping peak that correlates well with the discontinuous jump in the static stability at $M = 0.9$. (Compare Figs. 12 and 14.) The slight shift in the angle of attack between the undamping peak and the static stability jump results from failure of the small end plate on the dynamic model (Fig. 9) to completely eliminate spanwise flow. Oilflow photographs, taken of the dynamic model at discrete static angles of attack, verify the sudden merging of the channel flow shocks (Fig. 15), which caused the static stability jump (Fig. 12) and associated undamping (Fig. 13).

The stabilizing static stability jump constitutes an infinite, statically stabilizing derivative that, because of the flowfield time lag, produces an infinite destabilizing damping derivative for infinitesimal amplitude oscillations. As the oscillation amplitude grows, the effect of the discontinuity diminishes as it is balanced by the positive damping that surrounds the discontinuity.[13] Thus the undamping peak is amplitude sensitive, and the elastic cable tray will achieve a limit cycle at an amplitude where the effective aerodynamic undamping equals the structural damping.[11]

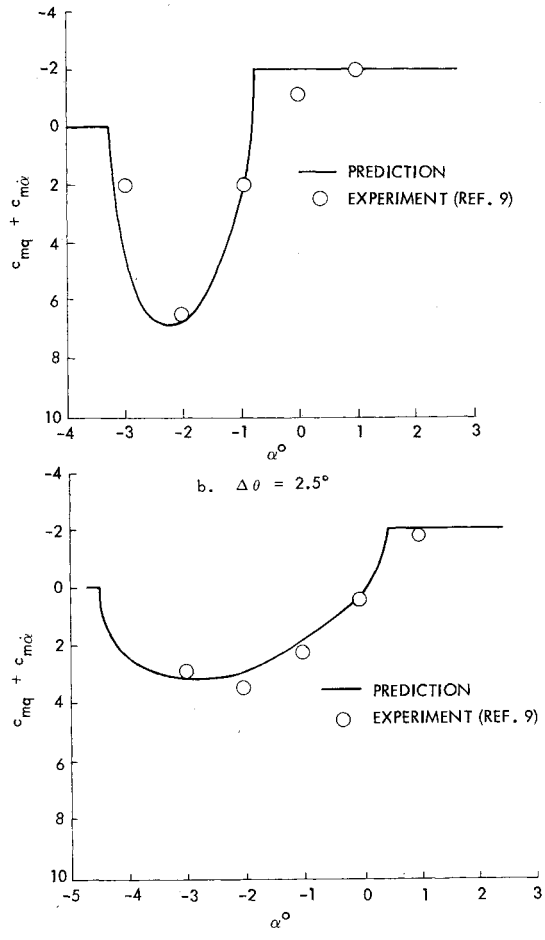

Fig. 17 Comparison between predicted and measured damping of the LO_2 cable tray at $M=0.92$.

Besides the undamping caused by discontinuous flow phenomena, the cable trays also experience undamping caused by continuous flow processes (Fig. 16). At subsonic speed, the flow in the channel under the cable tray is greatly accelerated, causing the separation bubble to close on the cable tray bottom. The flow reattachment creates a positive pressure region aft of the rotation center that generates a statically stabilizing but dynamically undamping moment on the tray. The topside of the tray is completely ineffective because it is totally submerged in a gross separated flow region. (See inserted sketches in Fig. 16.)

Gradually, the bottom-side separation bubble shrinks with increasing Mach number until, at $M=0.7$, the bottom-side corner flow becomes supersonic and the double shock system forms in the channel. Initially, the shocks are forward of the rotation center and are statically destabilizing and damping. As the Mach number is increased, the aft shock moves aft of the rotation center, and its effect becomes statically stabilizing and undamping.

The effect of changing span alters the Mach number where the double shock systems occur, verifying the existence of some spanwise flow in the dynamic test. Rounding the corners increases the undamping at low Mach number by allowing more movement of the separation bubble as the cable tray oscillates. Rounding the corners also causes a more gradual formation of the double shock systems.

Another important use of the dynamic data is to verify the prediction technique to be applied to the elastic cable tray; i.e., the method must successfully predict the rigid body dynamic data before one can confidently apply it to the elastic cable tray. The experimental results[6] in Fig. 17 are compared to the predicted damping derivatives[11,13] for the LO_2 cable tray at $M=0.92$ as a function of angle of attack (α) and

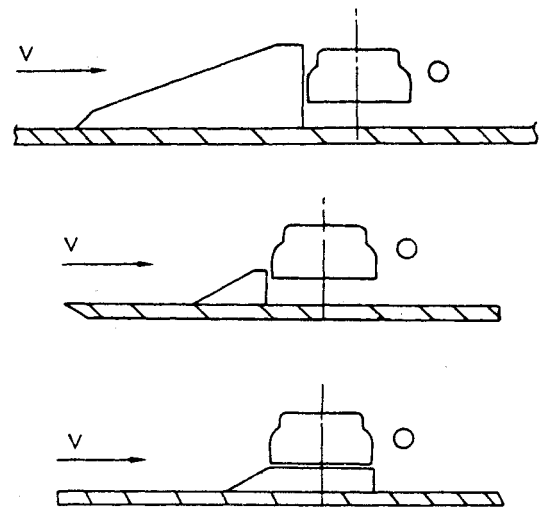

Fig. 18 Fixes tested.

oscillation amplitude ($\Delta\Theta$). The agreement is excellent. These computations assume an attached flow damping derivative equal to one-half the thin airfoil damping (because the topside flow on the cable tray is separated), adjusted for compressibility effects. The magnitude at the shock jump is determined from the static moment data (Fig. 12). The nondimensional time lag $\Delta\tau$ was taken to be

$$\Delta\tau = V/\bar{V}_d + V/V_u$$

where V_u, the upstream shock velocity, is assumed to be equal to the speed of sound, and the downstream mean convection velocity ($\bar{V}_d$) is one-half the local cross-flow velocity (V) as indicated by the static pressure data.[5,11]

The curvature of the LO_2 tank puts the LO_2 tray initially at $\alpha=3$ deg, thus causing it to experience the limit cycle oscillations associated with the shock jump phenomenon. There is no guarantee that the SRB tray will not also achieve a critical angle of attack locally at some combination of angle of attack and yaw angle. Thus it is quite possible that both the LO_2 and SRB cable tray will experience aerodynamic undamping. Whether this will cause excessive limit cycle oscillations must be determined by an aeroelastic analyses to which these tests furnish the required input.[11]

The Fix

Because of the fabrication lead time requirements, action had to be taken to eliminate the possibility of cable tray failure immediately upon completion of the wind tunnel tests. There was no time to complete the aeroelastic analysis. Three potential fixes had been tested dynamically: the ramp, the miniramp, and the gap filler (Fig. 18). The ramp and the gap filler had also been tested statistically. The ramp essentially submerged the cable tray in a separated wake, nearly eliminating all static and dynamic loads. The gap filler caused excessive static loads, and the gap had to be nearly constant along the entire chord to eliminate dynamic effects.[11] The miniramp, while nearly eliminating dynamic effects, showed some small undamping depending upon its standoff in front of the cable tray. Thus the ramp was the only completely acceptable fix that could be devised without further testing or analysis.

The LO_2 and SRB cable trays really required protection. The need for protection of the LH_2 tray was not clear. Certainly, in the outflow region ($\gamma<0$ in Fig. 6), the tray would be shielded by the LOX feed lines and other plumbing (Figs. 5 and 6). In the inflow region, however, the picture was less clear, especially because of the undamping effects of the

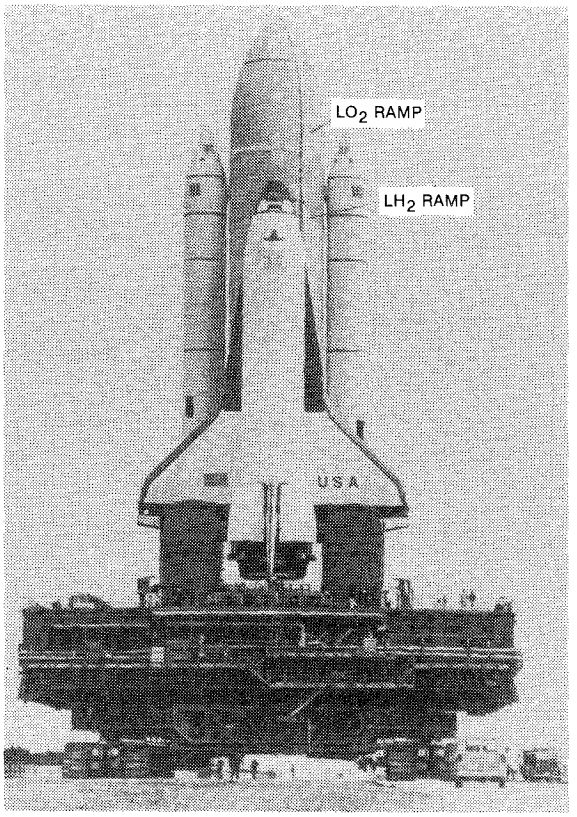

Fig. 19 Columbia booster.

small gaps of the gap filler. Thus the prudent course was taken, and the LH_2 tray was supplied with a shielding ramp over the inflow region along with the LO_2 and SRB trays. The LO_2 ramp and part of the LH_2 ramp are visible in the photograph of the Columbia booster ready for launch (Fig. 19).

It is interesting to note that the subsequent completion of the aeroelastic analysis[11] showed the LO_2 and SRB trays to experience aeroelastic instability leading to failure. Therefore, they needed the protection of the shielding ramps. However, the issue of the LH_2 tray was still in doubt after the analysis. Thus further testing at the proper gap and flow angles are needed to settle this issue.

Concluding Remarks

An analysis of static and dynamic wind tunnel data of the Shuttle cable trays has indicated that the LO_2 and SRB trays, and possibly the LH_2 trays, were in danger of experiencing aeroelastic instability leading to structural failure. This was prevented by the timely installation of protective wedge-shaped windshields. As is often the case in engineering, the decision to install the windshields had to be made before their need could be conclusively determined. However, subsequent analysis proved that their installation was necessary.

The real lesson lies in the need for any fix at all. Had the possibility of aeroelastic instability of the cable trays been considered from the outset of their design, the trays might have had a much different configuration, and no fix would have been necesssary. Thus, once again, the need for aeroelastic analysis early in the design phase has been demonstrated.

Acknowledgment

This paper is based upon results obtained from work done under contract to Martin-Marietta Corporation, Michoud Operations, New Orleans, La., with D.B. Schwartz as the contract coordinator.

References

[1] Ericsson, L.E. and Reding, J.P., "Analysis of Flow Separation Effects on the Dynamics of a Large Space Booster," *Journal of Spacecraft and Rockets,* Vol. 2, July-Aug. 1965, pp. 481-490.

[2] Reding, J.P. and Ericsson, L.E., "Aeroelastic Stability of the 747/Orbiter," *Journal of Aircraft,* Vol. 14, Oct. 1977, pp. 988-993.

[3] Reding, J.P. and Ericsson, L.E., "Effects of Flow Separation on Shuttle Longitudinal Dynamics and Aeroelastic Stability," *Journal of Spacecraft and Rockets,* Vol. 14, Dec. 1977, pp. 711-718.

[4] Ericsson, L.E. and Reding, J.P., "Aeroelastic Instability of Space Shuttle Protuberances," Paper 81-1672 presented at the AIAA Aircraft Systems Conference, Dayton, Ohio, Aug. 11-13, 1981.

[5] Michna, P.J. and Parker, D.R., "Test Results from the Pressure Test of a 0.12 Scale Model of the External Tank LO_2 Cable Tray and GO_2 Pressure Line and a 0.1575 Scale Model of the Aft ET/SRB Cable Tray in the MSFC 14-in. Trisonic Wind Tunnel Test No. TWT 661," Rept. MMC-ET-SE05-89, May 1980, Martin-Marietta Corporation, Michoud Operations, New Orleans, La.

[6] LaBerge, J.G., "Dynamic Wind Tunnel Tests of the Shuttle External Tank Cable Trays at Subsonic Speeds," LTR-UA-55, Aug. 1980.

[7] Carroll, W.R., "Trip Report 4-6 February to Present Cable Tray Aero Environment to MSFC, JSC, and RI/D and Plan Pilot Tests in MSFC 14-in. TWT," Martin Marietta Interoffice Memo. 3552-79-07, Feb. 12, 1979.

[8] Nakamura, Y. and Mizota, T., "Aerodynamic Characteristics and Flow Patterns of a Rectangular Block," Reports of Research Institute for Applied Mechanics, Kyusha University, Japan, Vol. XIX, No. 65, March 1972.

[9] LaBerge, J.G., "Effect of Flare on the Dynamic and Static Moment Characteristics of a Hemispheric-Cylinder Oscillating in Pitch at Mach Numbers from 0.3 to 2.0," Aeronautical Rept. LR-295, National Research Council of Canada, Jan. 1961.

[10] Ericsson, L.E., "Aeroelastic Instability Caused by Slender Payloads," *Journal of Spacecraft and Rockets,* Vol. 4, June 1967, pp. 65-73.

[11] Ericsson, L.E. and Reding, J.P., "Aeroelastic Analysis of the Space Shuttle External Tank Cable Trays," LMSC D766543, Lockheed Missiles and Space Company, Inc., Sunnyvale, Calif., April 1981.

[12] Ericsson, L.E., "Dynamic Effects of Shock-Induced Flow Separation," *Journal of Aircraft,* Vol. 12, Feb. 1975, pp. 86-92.

[13] Ericsson, L.E. and Reding, J.P., "Separated Flow Dynamics of Space Shuttle Cable Trays," Paper 81-1880, presented at the AIAA Atmospheric Flight Mechanics Conference, Alburquerque, N. Mex., Aug. 19-21, 1981.